



ELSEVIER

Contents lists available at SciVerse ScienceDirect

Optics Communications

journal homepage: www.elsevier.com/locate/optcom

Circular dichroism in planar extrinsic chirality metamaterial at oblique incident beam

Seoungjun Lee^{a,*}, Zengbo Wang^{a,b}, Cheng Feng^c, Jiao Jiao^a, Ashfaq Khan^d, Lin Li^a^a School of Mechanical, Aerospace and Civil Engineering, University of Manchester, Manchester M13 9PL, UK^b Schools of Electronic Engineering, Bangor University, Dean Street, Bangor, Gwynedd LL57 1UT, UK^c Chemistry Department, University of Leicester, University Road, Leicester LE1 7RH, UK^d Department of Mechanical Engineering, NWFU University of Engineering and Technology, Peshawar 25000, Pakistan

ARTICLE INFO

Article history:

Received 3 May 2013

Received in revised form

10 July 2013

Accepted 11 July 2013

Available online 24 July 2013

Keywords:

Metamaterial

Chirality

Circular dichroism

Visible wavelength

ABSTRACT

We present a two dimensional planar extrinsic chirality metamaterial (2D-ECM) design that has strong circular dichroism (CD) in the visible spectrum range rather than usual near-infrared and terahertz range. The 2D-ECM is theoretically investigated by incident beam angles and meta-molecules unit sizes in visible spectrums. Physical mechanism was illustrated in figures of vector directions in electric field.

© 2013 Elsevier B.V. All rights reserved.

1. Introduction

Circular dichroism (CD) is characterized by the differential absorption of right circularly polarized (RCP) light and left circularly polarized (LCP) light, and is related to polarization effect which can determine optical activity [1,2]. Circular dichroism spectroscopy has been widely used to gain information about biomolecule, DNA [3–5] and organic compounds [6]. Nanoparticles obtained strong CD in the geometry and composition of a chiral molecule [7–9]. CD was observed in double layers [10], mutually twisted unconnected layers [11], and single-layered gold sawtooth gratings [12] of chiral planar metamaterials at near-infrared wavelengths. Using terahertz frequency, optical activity and coupling effects can generate and assist CD [13,14]. A three-dimensional chiral metamaterial of mutually twisted planar metal patterns generated giant CD in parallel planes due to negative index of refraction [15]. In non-chiral metamaterials, optimized unit cell structure can improve the peak point of CD [16], and elliptical nano-holes array allows to observe CD in visible spectrum [17]. In this paper, we report that two dimensional planar extrinsic chirality metamaterial (2D-ECM) can generate strong CD at visible spectrums using electric distribution of Floquet modes in CST (computer simulation technology) microwave studio software. The structure of the 2D-ECM contains a silver single layer structure

on a borosilicate glass substrate. The refractive index and extinction coefficient of silver is changed by wavelengths, and measured at visible wavelengths [18]. The dielectric material of a borosilicate glass (N-BK7) is used for a thick substrate, and the data of the refractive index is obtained [19].

2. Methods

The transmission of RCP and LCP can be mathematically defined in a 2×2 t -matrix as [20]

$$\begin{pmatrix} T_+ \\ T_- \end{pmatrix} = \begin{pmatrix} t_{++} & t_{-+} \\ t_{+-} & t_{--} \end{pmatrix} \begin{pmatrix} I_+ \\ I_- \end{pmatrix} \quad (1)$$

where ‘+’ and ‘-’ are symbols for RCP and LCP incident beams, respectively. The matrix is combined by transmission (T) and incident (I) beam. t_{++} and t_{--} correspond to the transmission amplitude of RCP (I_+) and LCP (I_-) incident beams. t_{+-} and t_{-+} are calculated by the conversion between RCP and LCP. The incident electric field (E^{in}) and transmission electric field (E^{out}) are related to the t -matrix, where LCP and RCP indicate subscripts + and – as defined [20]:

$$E_i^{out} = t_{ij} E_j^{in} \quad (2)$$

and the Circular dichroism (CD) of LCP and RCP is mathematically defined as [20,21]

$$CD = |t_{++}|^2 - |t_{--}|^2 \quad (3)$$

* Corresponding author. Tel.: +44 161 306 3816.

E-mail address: seoungjun.lee@postgrad.manchester.ac.uk (S. Lee).

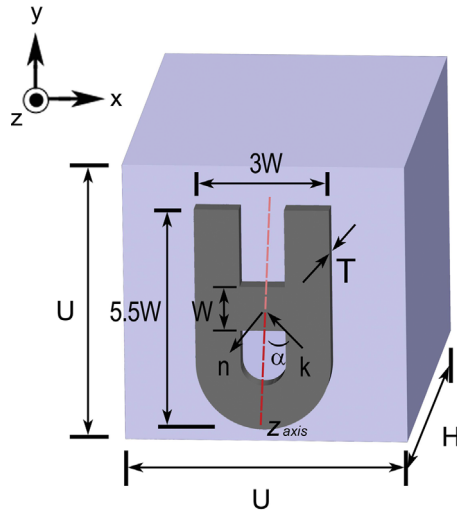


Fig. 1. Asymmetric unit cell structure ($U=250$ nm) of a borosilicate glass substrate ($H=1000$ nm) and silver unit cells ($T=20$ nm and $W=40$ nm). n is the direction of vector perpendicular to the unit cell. k is the direction of the incident beam, and emits along the relative x axis. α is angle of the incident beam, and is calculated by the direction of incident beam k to z axis.

$$CD = |T_{LCP}| - |T_{RCP}| \quad (4)$$

CD spectrum was simulated by modern finite integrate technique (FIT) in frequency domain. Different angles of oblique incident beams were applied in the unit cell. The spectrum was demonstrated and compared between LCP and RCP. The 2D-ECM design consists of unit cells of 20 nm thick silver layer on a 1000 nm thick borosilicate glass substrate as shown in Fig. 1. The borosilicate glass substrate is dielectric substrate which can help to break mirror symmetry so optical activity can be boosted [22]. At vertical incident beam ($\alpha=0^\circ$), it forms mirror image because the asymmetric unit cell structure has the same direction as incident beam so it is not 3D-chiral. However, at tilted incident beam ($\alpha \neq 0^\circ$), the asymmetric unit cell structure is transformed into extrinsically 3D-chiral as it is not mirror image between LCP and RCP [13]. The 2D-ECM forms unit cell boundary condition in x and y dimensions, and open boundary condition in z dimension. The unit cell boundary condition is quite similar to the periodic boundary condition but when open boundaries are perpendicular such as using waveguide ports, the unit cell boundary condition approaches Floquet modes. Oblique incident beams of LCP and RCP propagates into z dimension using waveguide ports. The waveguide ports support to calculate returning power using S-parameters.

3. Results and discussion

Fig. 2 shows CD spectrum of the 250 nm unit cell in wavelengths between 450 nm and 800 nm at various incident angles of $\alpha=0^\circ, \pm 20^\circ, \pm 71^\circ$ and $\pm 80^\circ$. In wavelengths below 610 nm, the spectrum curves are highly oscillating. This is because of strong optical diffraction associated with the unit cell [20], which may lead to disturbance and diffraction of the oblique incident beams in the layer of the unit cell. Above 610 nm wavelengths, the spectrum curves change smoothly because the optical diffraction is negligible. The maximum CD peaks were 0.4914 at 726.39 nm visible wavelength occurring at angles $\alpha=71^\circ$, where is the highest difference between LCP and RCP. It shows that 71° tilted incident beams of LCP and RCP may have distinctive interactions between electric and magnetic dipoles, which may generate most clear optical activity. CD did not appear at 0° oblique incident beams because the projection of electric and magnetic moment

is symmetrically the same between LCP and RCP [23]. It means that the location and magnitude of electric and magnetic dipoles could be the same. The $\pm 20^\circ, \pm 71^\circ$ and $\pm 80^\circ$ were intersected

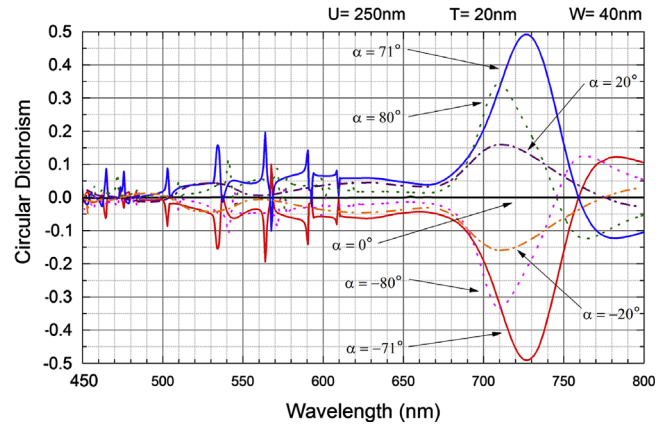


Fig. 2. Comparison of CD in the 250 nm unit cell between different incident beam angles as $\alpha = \pm 80^\circ, \pm 71^\circ, \pm 20^\circ$ and 0° at wavelengths (λ) between 450 nm and 800 nm. The maximum CDs are in Table 1.

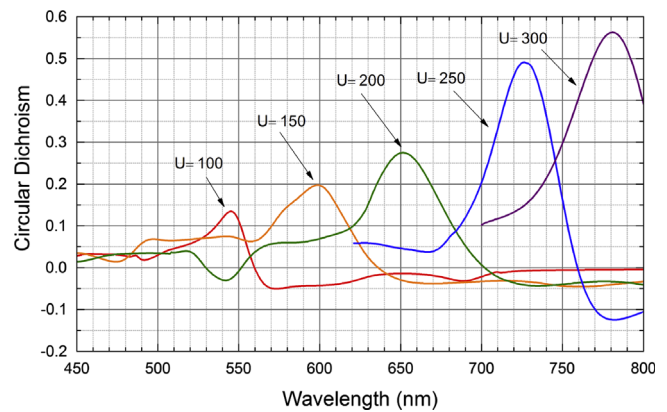


Fig. 3. Dependence of CD on the wavelengths (λ) between 450 nm and 800 nm for 100 nm unit cell with $\alpha=77^\circ$, 150 nm unit cell with $\alpha=58^\circ$, 200 nm unit cell with $\alpha=45^\circ$, 250 nm unit cell with $\alpha=71^\circ$, and 300 nm unit cell with $\alpha=57^\circ$. The maximum CDs are in Table 2. Highly oscillated curves are removed in $U=250$ and 300.

Table 1

aaaaa250 nm unit cell with various angles, wavelengths and CD.

Angle (α , deg)	Optimized wavelength (λ , nm)	Transmission spectrum (CD)
0	It does not appear	It does not appear
20	710.90	0.1602
71	726.36	0.4914
80	710.06	0.3438

Table 2

Different sizes of unit cells with optimized angles, wavelengths and CD.

Unit cell size (U , nm)	Optimized angle (α , deg)	Optimized wavelength (λ , nm)	Transmission spectrum (CD)
100	77	545.45	0.1345
150	58	598.80	0.1976
200	45	651.47	0.2750
250	71	726.36	0.4914
300	57	781.25	0.5627

and no CD value at 770 nm, 760 nm, and 740 nm wavelengths, respectively. At intersected wavelength points, the magnitude of LCP and RCP could be quite similar so CD was not generated. In addition, three different angles of CD can have similar curve

Table 3
Different widths of 250 nm unit cell with optimized angles, wavelengths and CD.

Width (W)	Optimized angle (α , deg)	Optimized wavelength (λ , nm)	transmission spectrum (CD)
24	63	599.63	0.1878
28	55	621.30	0.2635
32	45	650.05	0.2762
40	71	726.36	0.4914

patterns but the peak and intersected position were various. It might cause optical activity with particular oblique incident beams. Different wavelengths of oblique incident beams can determine different locations of electric and magnetic dipoles while k vector penetrates into the extrinsically 3D-chiral.

A comparison between 100 nm, 150 nm, 200 nm, 250 nm, and 300 nm unit cells is presented in Fig. 3. It demonstrates that the different sizes of unit cells can determine the peak position of a wavelength and magnitude of CD. When the unit cell size is shrunk, the maximum CD is decreased and the peak wavelength is shifted to smaller wavelengths. Otherwise, increasing unit cell size generates the reverse effect. The effects may cause different electric and magnetic moments on the surface of the 2D-ECM. The bigger unit cell (U) and wider structure (W) can generate

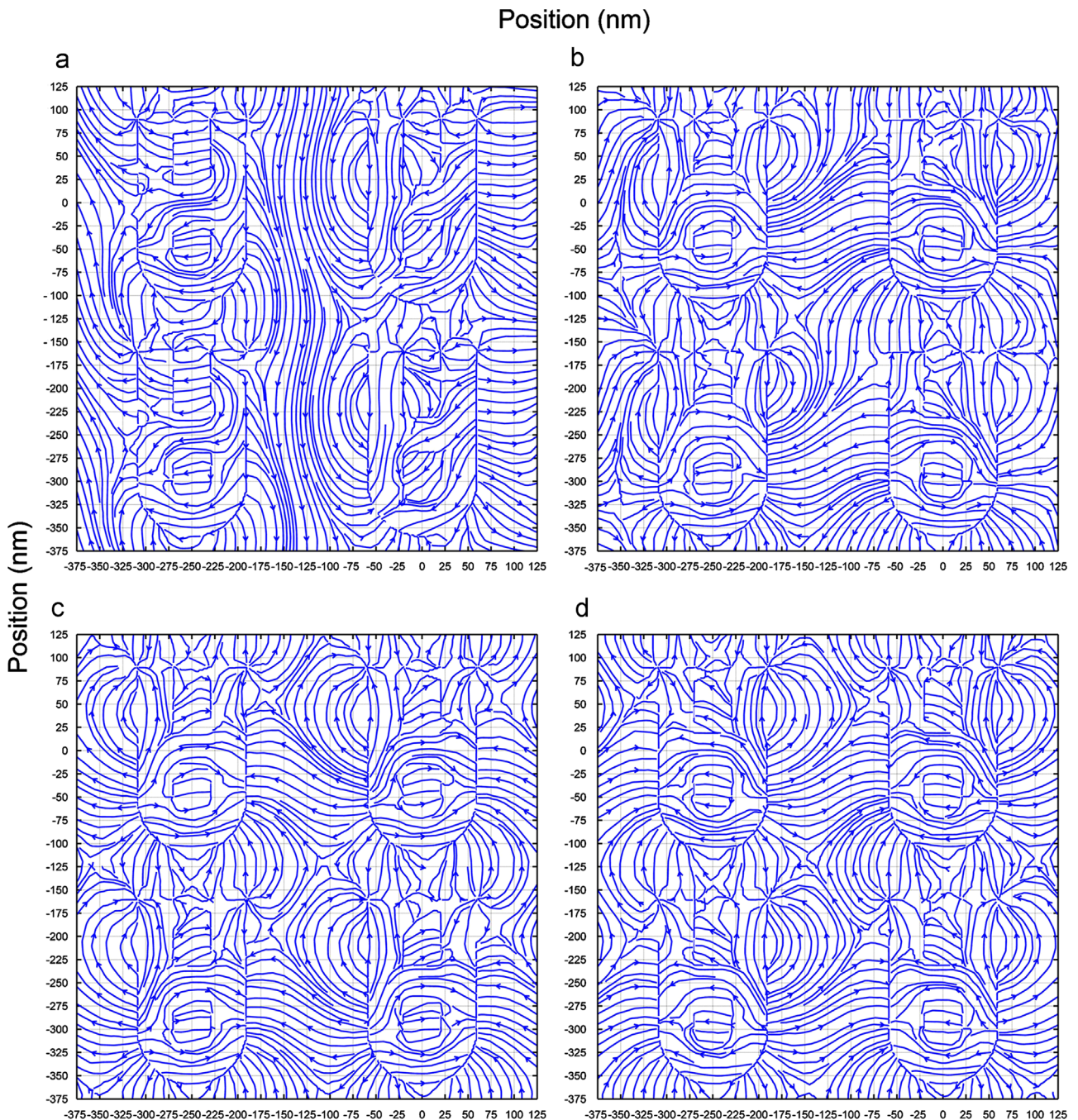


Fig. 4. Electric field with streamline and vector direction in the 250 nm unit cell boundary condition using Floquet modes with 1000 nm height of borosilicate glass substrate, $T=20$ nm thickness, and $W=32$ nm width of silver at (a), (b) $\alpha=71^\circ$ and (c), (d) 0° of incident beam, with $\lambda=726.36$ nm between LCP and RCP.

higher electric and magnetic energies because the optical activity can have more active resulting in the electric and magnetic dipoles. Furthermore, the position and power of magnetic and electric dipoles may be relocated at diverse angles of oblique incident beams. As a result, the magnitude of LCP and RCP is not the same in the 2D-ECM. The 300 nm unit cell has the biggest CD but it is out of the visible spectrum so the 250 nm unit cell has the biggest CD in visible spectrum. Various unit cell sizes with Maximum CDs and these of diverse angles are presented in Table 2. It is an agreeable result that the 2D-ECM can generate giant CD compared to planar chiral split-ring metamaterials ($CD=0.04$ in GHz) [21] and planar non-chiral elliptical nano-holes array metamaterials ($CD=0.12$ in visible spectrum) [17]. The 100 nm, 150 nm, 200 nm, 250 nm, and 300 nm unit cells have the optimized angles at $\alpha=77^\circ$, 58° , 45° , 71° , and 57° , respectively. Optimized angles are dependent of unit cell sizes because the electric and magnetic dipoles may be located in different positions, so different forces of optical activity may be generated in the varied unit cells. The 250 nm unit cell is demonstrated with varied width of the ECM in Table 3. It includes maximum CDs, that of an angle and a wavelength. It shows that optimized unit cell structure can control a peak and that of a wavelength of CD. The maximum CDs are 0.1878, 0.2635, 0.2762, and 0.4914 at $W=24$, 28, 32, and 40, respectively. The narrow width can shrink the total size of silver unit cells so that the area of dipoles may be diminished. As a result, the wavelength of maximum CDs can be determined by unit cell size, and the bigger unit cell size can shift to higher wavelength. The area of the 2D-ECM can affect the wavelength of CD and CD value. The larger area could have strong CD but the wavelength of CD could be also increased. Strong optical activity may not generate in the narrow width and small size of unit cells as it may reduce the energy of surface plasmon on the 2D-ECM. Thus, $U=250$ and $W=40$ can be optimized CDs in visible spectrum.

A comparison of LCP and RCP is presented in electric field using CST raw data with Matlab coding as shown in Fig. 4. 71° tilted and vertical incident beam was applied in electric field. The four unit cells were monitored simultaneously between LCP and RCP. In the vertical incident beam (0° oblique incident beam), the LCP states of unit cells are symmetrically opposite to that of RCP. It means that the electric interaction of unit cells is almost same between LCP and RCP so optical activity did not appear in CD spectrum. In 71° tilted incident beam, the distribution of positive and negative charges is different in LCP and RCP. Such as the row of unit cells is quite same but the column of unit cells has different locations in positive and negative charges. As a result, CD is obtained by trapped energy in resonance during polarization conversation [24]. The electric interaction between LCP and RCP can generate different electric flows in the unit cells. Thus, giant CD can be generated by the different energy distribution between LCP and RCP in tilted incident beams. It can be also related to different magnitudes of CD, and that of an optimized angle and a wavelength. Furthermore, The unit cell structure can affect actual coupling aspects [25] so the interaction between neighboring unit cells may cause main reason of strong CD.

4. Conclusions

In visible spectrum, we show that the 2D-ECM can have strong CD at angled incident beam due to critical interactions between positive and negative charges in LCP and RCP. The strong CD may be obtained by different neighboring interactions of unit cells between LCP and RCP. In vertical incident beam, CD is not generated because the interactions of unit cells are identically same as LCP and RCP. The size of unit cell (U) and width (W) can increase the wavelength and magnitude of CD but it will lead out range of visible spectrum. The CD of the 2D-ECM is significantly affected by incident beam angles and meta-molecules unit sizes. Moreover, such strong CD can open up bio-molecular detecting systems and vibration sensors at visible spectrums because the detecting system works better with strong CD. Thus, sensitive biological samples may be applied in the 2D-ECM such as the identification of DNA or virus.

References

- [1] C. Menzel, C. Rockstuhl, F. Lederer, *Physical Review A: Atomic, Molecular, and Optical Physics* 82 (2010).
- [2] S.N. Volkov, K. Dolgaleva, R.W. Boyd, K. Jefimovs, J. Turunen, Y. Svirko, B. K. Canfield, M. Kauranen, *Physical Review A—Atomic, Molecular, and Optical Physics* 79 (2009).
- [3] S. Paramasivan, I. Rujan, P.H. Bolton, *Methods* 43 (2007) 324.
- [4] L. Whitmore, B.A. Wallace, *Biopolymers* 89 (2008) 392.
- [5] N.J. Greenfield, *Nature Protocols* 1 (2006) 2876.
- [6] N. Berova, L.D. Bari, G. Pescitelli, *Chemical Society Reviews* 36 (2007) 914.
- [7] Z. Fan, A.O. Govorov, *Nano Letters* 10 (2010) 2580.
- [8] J. George, K. George Thomas, *Journal of the American Chemical Society* 132 (2010) 2502.
- [9] A.O. Govorov, Z. Fan, P. Hernandez, J.M. Slocik, R.R. Naik, *Nano Letters* 10 (2010) 1374.
- [10] D.H. Kwon, P.L. Werner, D.H. Werner, *Optics Express* 16 (2008) 12802.
- [11] E. Plum, V.A. Fedotov, A.S. Schwanecke, N.I. Zheludev, Y. Chen, *Applied Physics Letters* 90 (2007).
- [12] W. Gao, C.Y. Ng, H.M. Leung, Y. Li, H. Chen, W.Y. Tam, *Journal of the Optical Society of America B: Optical Physics* 29 (2012) 3021.
- [13] R. Singh, E. Plum, W. Zhang, N.I. Zheludev, *Optics Express* 18 (2010) 13425.
- [14] M. Decker, R. Zhao, C.M. Soukoulis, S. Linden, M. Wegener, *Optics Letters* 35 (2010) 1593.
- [15] E. Plum, J. Zhou, J. Dong, V.A. Fedotov, T. Koschny, C.M. Soukoulis, N. I. Zheludev, *Physical Review B—Condensed Matter and Materials Physics* 79 (2009).
- [16] C. Feng, Z.B. Wang, S. Lee, J. Jiao, L. Li, *Optics Communications* 285 (2012) 2750.
- [17] T. Cao, M.J. Cryan, *Journal of Electromagnetic Waves and Applications* 26 (2012) 1275.
- [18] E.D. Palik, *Handbook of Optical Constants of Solids*, Academic Press, Boston, 1985.
- [19] *Optical Glass Data Sheets*, Schott, 2013.
- [20] E. Plum, X.X. Liu, V.A. Fedotov, Y. Chen, D.P. Tsai, N.I. Zheludev, *Physical Review Letters* 102 (2009).
- [21] A.V. Novitsky, V.M. Galynsky, S.V. Zhukovskiy, *Physical Review B—Condensed Matter and Materials Physics* 86 (2012).
- [22] S.I. Maslovski, D.K. Morits, S.A. Tretyakov, *Journal of Optics A: Pure and Applied Optics*, 11, , 2009.
- [23] E. Plum, V.A. Fedotov, N.I. Zheludev, *Journal of Optics A: Pure and Applied Optics* 11 (2009).
- [24] S.V. Zhukovskiy, A.V. Novitsky, V.M. Galynsky, *Optics Letters* 34 (2009) 1988.
- [25] J. Petschulat, A. Chipouline, A. Tünnermann, T. Pertsch, C. Menzel, C. Rockstuhl, T. Paul, F. Lederer, *Physical Review B—Condensed Matter and Materials Physics* 82 (2010).